Construction and Control of an Air-Cored Permanent Magnet Linear Generator for Direct Drive Wave Energy Converters

Rieghard Vermaak[1], *Member IEEE*, and Maarten J. Kamper[2], *Senior Member IEEE*
Department of Electrical and Electronic Engineering
University of Stellenbosch
Stellenbosch, South Africa
[1]rvermaak@ieee.org, [2]kamper@sun.ac.za

***Abstract*— Direct drive wave energy converters using linear generators are attractive due to their high efficiency and reliability. Air-cored generators in particular are receiving increasing attention due to the elimination of attraction forces between the stator and translator and the resulting reduction in structural mass. In this paper, details of the construction of a novel air-cored linear generator are presented. A custom test rig is constructed for testing the generator, particularly with zero overlap between its stator and translator at the stroke ends. Predictive control for maximum power transfer from the generator is first proposed and tested as an alternative to methods employing linear position feedback and EMF estimation with sense coils. The control strategy is demonstrated to work correctly and it is shown that zero overlap at the stroke ends improves power generated per translator mass compared to complete stator-translator overlap during the entire stroke.**

Keywords-Air-cored; direct drive; linear generator; predictive control; wave energy.

I. INTRODUCTION

The earth's oceans contain a massive amount of clean and sustainable energy in the form of its waves. Of all the different wave energy converters (WECs) that are currently being investigated, no superior technology is yet apparent though [1]; it is as such that commercial-scale wave energy is not yet a reality and that continued research in the field is necessary. Most WECs have some kind of primary mechanical interface which captures the wave energy. An intermediate power conversion stage, called the power take-off (PTO), converts this captured energy to a form suitable for driving a conventional electrical generator. The PTO is usually a pneumatic or hydraulic system. Energy storage mechanisms in the form of hydraulic accumulators or flywheels are used for smoothing of the variable energy captured from the waves. In many cases a power converter at the generator output is also needed to further smooth out the power fed to the grid.

A technology which does stand out from the others in one aspect is direct drive (DD) WECs. DD-WECs try to eliminate the PTO in order to reduce maintenance requirements and to increase reliability and efficiency; this makes it a very attractive option for the harsh environment of the ocean. With DD-WECs, the heave motion of the waves is used to directly drive a linear generator (LG). A well known example of such a device is the Archimedes Wave Swing (AWS) [2]. Some other DD-WECs in development can also be seen in [3]-[5]. The LG output varies in amplitude, frequency and phase sequence due to the reciprocating motion of the WEC and the lack of inherent energy storage mechanisms. Some research focuses on LGs without application to a specific WEC, e.g. [6]-[9].

Due to this variation in the LG output, power electronic converters with enough energy storage on the dc-bus are essential for connecting the LG output to the grid. Aggregation of phase shifted outputs of multiple LGs however relaxes the energy storage requirements as a natural smoothing effect occurs [10], [11]. Using power converters also comes with added benefits though. Voltage source converters (VSCs) are for instance an excellent grid interface in terms of complying with grid codes [12]. On the generator side a converter provides control of the generator current such that maximum power can be extracted from the WEC. Much research has addressed the issue of maximum power extraction from DD-WECs [9], [13]-[17] and is also part of the focus of this paper.

Testing of LGs and their converters in the laboratory is not straightforward as linear drive systems are not commonplace in traditional electrical machines laboratories. Custom test rigs were for instance developed for laboratory testing of linear generators in [4], [7], [9], [14] and [17]. This includes vertical [4] and horizontal [7] hydraulic drive systems, cable-and-pulley systems [9], [14] and a VSD with a worm-and-ball gear [17]. Control hardware and software for such drive systems are also needed to simulate wave motion under a varying generator load. Developing a drive system for testing linear generators can thus become a project on its own with considerable cost.

The authors of this paper developed a novel air-cored permanent magnet (PM) LG for use in DD-WECs. Details of the design are given in [8]. More detail regarding the construction of the LG is given in this paper in Section II. A new laboratory test system is developed for the LG (Section III) which allows testing of the proposed predictive control strategy (Section IV) for the generator output. Simulation and test results are presented in Section V and VI respectively.

The financial assistance of the South African National Energy Research Institute towards this research is hereby acknowledged. Opinions expressed and conclusions arrived at, are those of the author and are not necessarily to be attributed to SANERI.

II. EXPERIMENTAL LINEAR GENERATOR

A. Background

Because the heave motion of waves is rather slow (1 – 2 m/s peak) [17], the LGs in DD-WECs need to react very large forces in order to generate a significant amount of power. The LGs therefore become very large and expensive. The LGs of the AWS [2], Uppsala University [5] and Oregon State University [4], which are among the few which have been tested in the sea, are all of the iron-cored longitudinal flux (LF) type. Because the LGs are so large, the attractive forces between the PM translator and iron-cored stators are also very large and pose significant challenges in terms of bearing design and construction of the machine. Structural material for supporting these attractive forces also contributes significantly to the WEC's overall cost. Cogging forces, especially due to pair-wise flux coupling and the longitudinal ends of iron-cored generators, also cause problems [4], [18].

Due to the above named issues, air-cored machines are receiving increasing attention for use in DD-WECs [3], [6]-[8], [17]. Despite using more PM material than a comparable iron-cored machine, the elimination of cogging forces and the elimination of the attraction forces between the stator and translator make air-cored generators worth the while in this case. Trident Energy UK uses a tubular air-cored LG in its WECs [3]. A similar generator is investigated in [6], [17]. At Edinburgh University, a novel linear double-sided (LDS) PM translator air-cored topology named the C-Gen is currently being developed [7]. By using a LDS PM translator, a higher air gap flux density than in a single-sided air-cored machine, can be maintained. However, attractive forces between the two opposing translator sides are now introduced which again creates the need for increased structural mass.

B. The novel air-cored PMLG

The authors developed a novel air-cored topology from the LDS machine and this is shown in Fig. 1(a). The topology evolved by placing a number of LDS machines in a tubular topology, removing the iron yokes and merging adjacent magnets. The flux from any magnet now circulates transversely around the machine while each magnet experiences an ideally equal force from either side (i.e. the net force is ideally zero). The effect is that very little structural material is needed for PM support. The stator consists of a number of separate sections which are inserted between the PMs. The design and optimization of the machine is reported on in [8]. More details on the construction of a 1 kW prototype are given here.

Each separate stator section consists of non-overlapping concentrated coils cast into epoxy resin for support. Sixteen strands of 0.5 mm copper wire were twisted together to form a litz-wire; this limits the eddy-current losses in the copper wire. The litz-wire was then wound around a former to create the preformed coils, as shown laid-up in a mold in Fig. 1(b). Epoxy resin was cast around three of the preformed coils (for three phases) to form a finished stator section, as shown in Fig. 1(c). The completed stator, as seen in Fig. 1(d), consists of 38 of these sections bolted to the inside of an aluminium ring. The winding and casting was by far the most labor and time intensive process in the construction of the machine.

The translator was constructed from layers of engineering plastic and thinner layers of non-magnetic stainless steel pressed over a square steel pipe. These layers can be seen in the CAD drawing in Fig. 1(a) and are also shown close-up in Fig. 2(a). The plastic forms the non-magnetic spacers between the magnets and the stainless steel serves as a more rigid non-magnetic support for the PMs. The PMs, as shown in Fig. 2(b), are slightly tapered and have grooves at the top and bottom for the stainless steel to slide into; they were therefore simply slid into place from the outside. Assembling the translator was easy and fast compared to the stator construction.

For LGs, the PM translator is usually made to be longer than the stator, otherwise part of the stator would become inactive during the stroke and only contribute toward copper losses. The same approach was followed here. The translator was made twice as long as the stator. It was planned that the translator would however still move beyond the ends of the stator in order to investigate the effect of this on the output and the control strategy. Finite Element (FE) simulation results in Fig. 3(a)

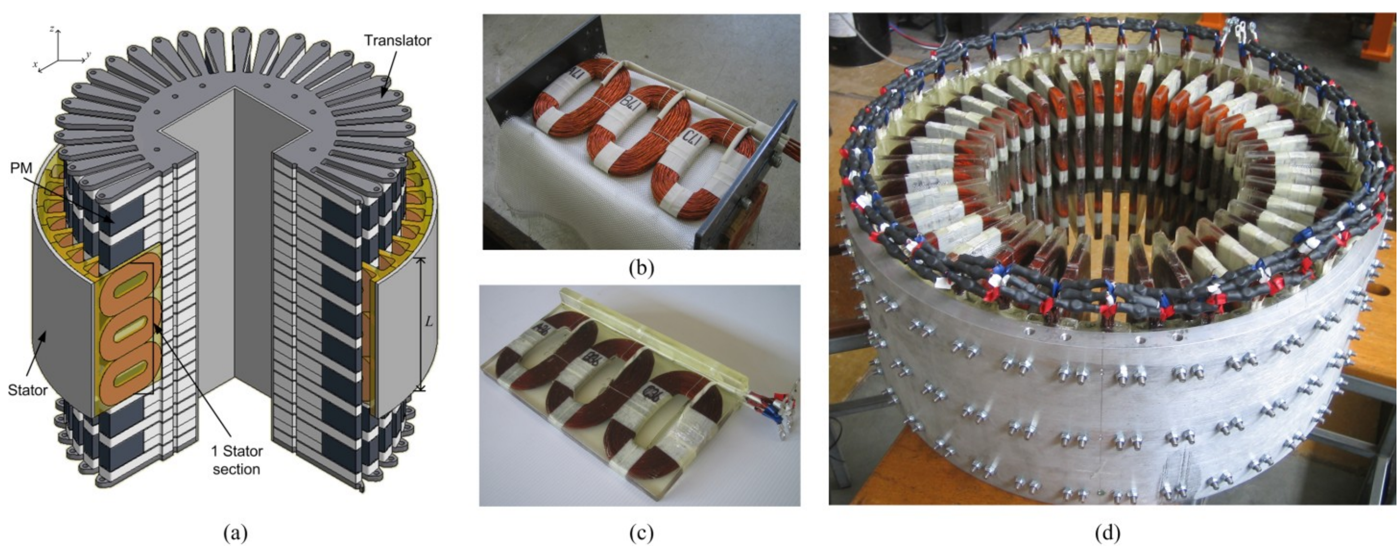

Fig. 1 (a) 3D cut-out view of the novel air-cored PMLG. (b) Three preformed coils as laid up in the mold and (c) the finished stator section after removing from the mold. (d) The completed stator consisting of 38 molded stator sections bolted to the inside af and aluminium ring and connected in series.

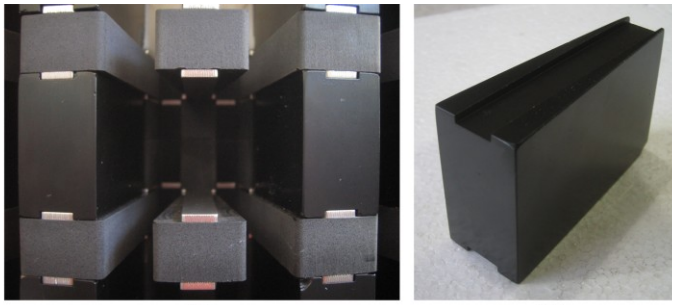

(a) (b)

Fig. 2 (a) A close-up of the translator with one PM removed; the layers of plastic (dull black) and stainless steel is evident. (b) One PM showing the tapered shape and the grooves at the top and bottom into which the stainless steel strips slide.

show the LG EMFs in the hypothetical case where the PMs covered the stator through the entire length of the stroke. The actual LG's simulated EMFs are shown in Fig. 3(b). If the per unit energy per PM mass from the hypothetical LG is taken as unity, the energy per PM mass of the real LG turns out to be 1.46 p.u. Although the length of this LG was not designed for a real sea state, this result shows that, from a cost perspective, it could make sense to allow for zero overlap between the stator and translator at the stroke ends. The loss of translator control will need to be taken into account though.

III. Test Setup

A schematic diagram of the chosen test setup for the linear generator is shown in Fig. 4. Since a relatively simple and cheap solution for a test rig was sought, use was made of existing equipment as far as possible. This entailed modifying and reusing an existing experimental 20 kW 40-pole PM wind turbine generator (WTG) and back-to-back IGBT VSCs which were used for grid-connection of the WTG.

The WTG was fitted with a crankshaft for converting its rotation to translation for driving the linear generator. The linear generator was mounted horizontally with its stator suspended on linear tracks (shown in Fig. 5). Since the stator is much lighter than the translator, it is easier to move the stator rather than the translator. The WTG was mounted with its axis vertical and its back plate was replaced with a slightly larger one to provide the required stroke length. The one VSC is used to drive the WTG as a motor and the other one is used as an active rectifier for the LG output. A LC-filter is used to smoothen the current produced by the modulated output voltage of the active rectifier. The energy in the system is effectively circulated through the motor, the LG and the dc-bus. A variable three-phase ac supply is used to charge up the dc-bus through a diode rectifier and also to feed the losses in the system. No provision is made for grid connection of the LG output. In a real wave power plant, the power from a number of DD-WECs will probably feed onto a common dc-bus from where it will then be inverted to the grid [10], [11]. Connecting the output from one LG to the grid is therefore deemed as an unnecessary exercise here.

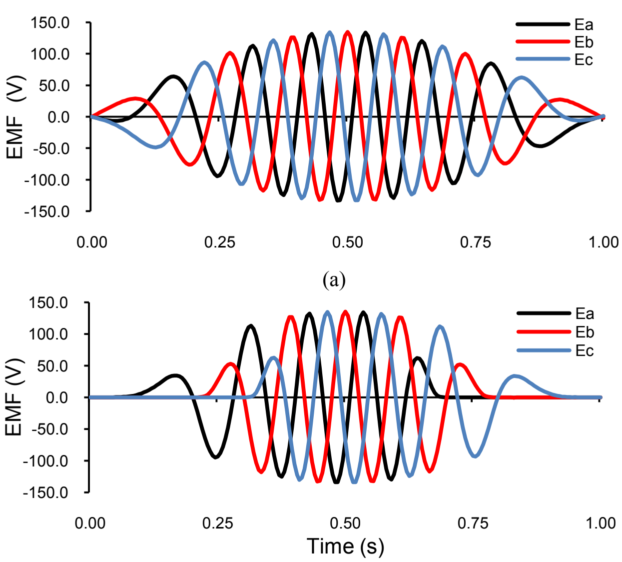

(b)

Fig. 3 FE simulated EMF of the generator with (a) the PM translator overlapping the whole stator during the entire stroke, and (b) with zero overlap between the translator and stator at the stroke ends.

IV. Power Conversion Control

A. Background

The energy conversion process in DD-WECs can be seen in terms of the mechanical energy absorbed from the waves by the front-end mechanical interface (e.g. the buoy) and the electrical energy absorbed from the LG by the load. The theory on energy absorption from the waves is covered in [1], [15]. Max-

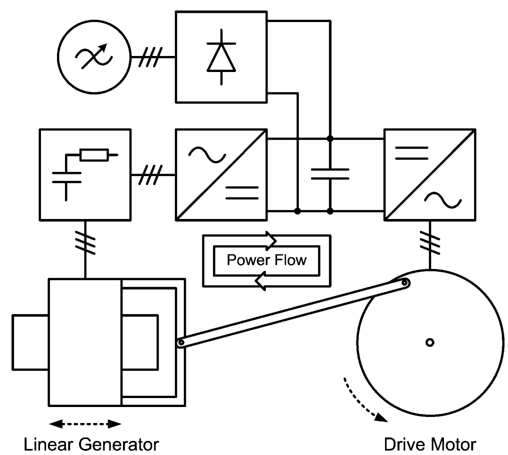

Fig. 4 Schematic representation of the generator and converter test setup.

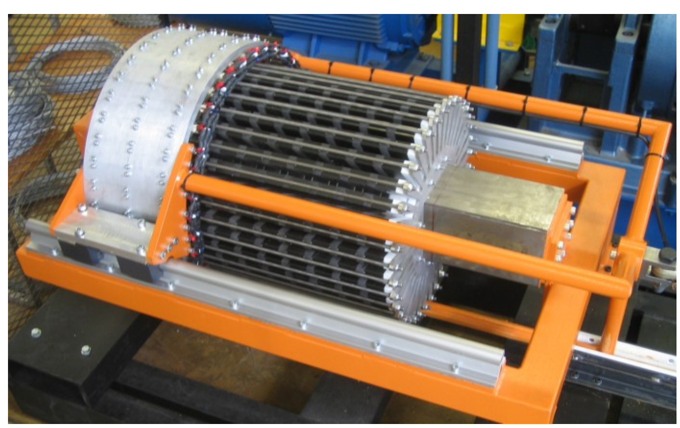

Fig. 5 Completed linear generator mounted horisontally on the test bench.

imum energy is captured from the waves when the device velocity is in phase with the wave force and with the device's damping force equal to that of the waves; this effectively constitutes a resonance condition between the waves and the device. This condition can be achieved by controlling the device's reaction to the waves with mechanical means (e.g. the AWS [2]) or electrically by manipulating the LG current with a power converter [9], [15], [16]. Maximum energy transfer between the LG and load likewise occurs with the current in phase with the EMF and with amplitude as given in (1) [13], [17].

Device reaction force control with a power converter has obvious advantages over mechanical actuators like in the AWS, e.g. faster operation, lower maintenance and greater flexibility. However, reaction force control will always cause a phase difference between the LG current and EMF as reactive power needs to be returned to the waves during part of the period [1], [9], [15]; the condition for maximum power transfer between the generator and load is therefore compromised.

As the LG of this paper is not device specific, optimal mechanical energy capture will be ignored here and the focus will only be on controlling power transfer between the LG and load.

B. Control Strategy

For maximum power transfer from a generator with EMF $e(t)$ and internal resistance R, the current $i(t)$ should be equal to

$$i(t) = e(t)/(2R), \qquad (1)$$

as also given in [17]. In this case, the copper losses in the generator will equal the transferred power, resulting in 50 % efficiency, which of course is not wanted. However, it is clear that, apart from being in phase with the EMF, the current should also be controlled to be proportional to the EMF; the scale factor will depend on the power available in the waves. The EMF can however not readily be measured while on load. In [13], [17] sense coils are used to determine the EMF amplitude and phase. The authors of [13] admit that this is a cumbersome practice and that sensorless methods should be investigated.

In this paper a predictive (or also known as a "dead-beat") control strategy, as discussed in [19], [20], is proposed for the LG current control. The principle of this inherently digital type of control is to calculate the converter voltage necessary to force the measured current to its reference value by the following modulation period [19]. Calculation of the converter voltage reference must be based on accurate knowledge of the system parameters such as resistance and inductance [19]. In the same way the EMF can also be calculated instead of being determined from sense coils. Once the EMF has been calculated, the reference current can be obtained from (1).

Space vector (SV) PWM, which is ideally suited to digital control, is used to generate the IGBT gating signals as discussed in [21]. For this, the measured current and voltages should first be transformed to the stationary two-coordinate $\alpha\beta$-reference frame (also explained in [21]) wherein all calculations should then be performed. This reduces the number of calculations performed compared to doing so in the *abc*-reference frame. Also, no position feedback (e.g. from a linear encoder as in [14]) is needed for transformation to the synchronously rotating *dq*-reference frame as done in [14], [16].

A single line diagram of the generator connected to the VSC through the LC-filter is shown in Fig. 6. In terms of the measured generator terminal voltage $v_t(t)$ and converter current $i(t)$, the average converter voltage $v_c(t)$ is given as

$$v_c(t) = v_t(t) - L_f \frac{di(t)}{dt}, \qquad (2)$$

where L_f is the filter inductance. Writing this as a difference equation for digital implementation gives

$$v_c[k] = v_t[k] - \frac{L_f}{T_s}\big(i[k+1] - i[k]\big), \qquad (3)$$

where T_s is the switching period. If the current error is given as $\varepsilon_i[k] = i^*[k] - i[k]$, the dead-beat condition gives $\varepsilon_i[k+1] = 0$ [20]. This means that $i[k+1]$ must equal the reference current $i^*[k]$. Substituting this into (3) then gives the converter voltage needed to achieve the deadbeat condition as

$$v_c^*[k] = v_t[k] - \frac{L_f}{T_s}\big(i^*[k] - i[k]\big). \qquad (4)$$

In the LG model shown in Fig. 6, the synchronous inductance L_s can be ignored; this is because the inductance of air-cored machines is low and also because the LG operates at low frequencies (up to 9.5 Hz). Now, assuming that only current at the switching frequency flows through the filter capacitor C_f, the EMF can be calculated as

$$e[k] = v_t[k] + i[k]R_s, \qquad (5)$$

where R_s is the generator phase resistance. From (1), the optimal reference current can now be calculated as

$$i^*[k] = k_o e[k] = \big[1/(2R_s)\big]e[k]. \qquad (6)$$

The control strategy is shown schematically in Fig. 7.

V. Simulation

The LG, filter and converter as shown in Fig. 6 was implemented in the multi-domain simulation package Ansys Simplorer® for verification. The data from the FE simulated EMFs shown in Fig. 3(b) is stored in a lookup table and used as reference for ideal voltage sources representing the LG EMFs. The VSC is modeled with ideal switches representing the IGBTs and an ideal dc voltage source is used to represent the dc-bus. The parameters as used in the simulation are given in Table I. Simplorer® includes a VHDL-AMS solver, and therefore the control and SV-PWM calculations were implemented with VHDL code as described in [22].

Fig. 8(a) shows the simulated currents injected to the converter during one stroke under optimal control. The current amplitudes deviate from the ideal sinusoidal envelope at the stroke ends; this can be expected when considering the EMFs of Fig. 3(b). In Fig. 8(b), the *c*-phase EMF, terminal voltage and current are shown. During the first part of the stroke, the *a*-phase and *b*-phase become active first. It can be seen that, since the three phase currents are balanced, current from the *a* and *b* phases are conducted through the *c*-phase before it becomes ac-

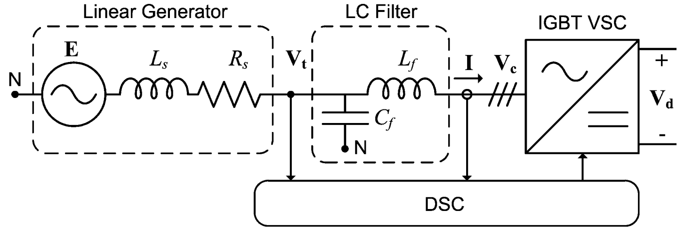

Fig. 6 Single line diagram of the LG, filter, converter and DSC.

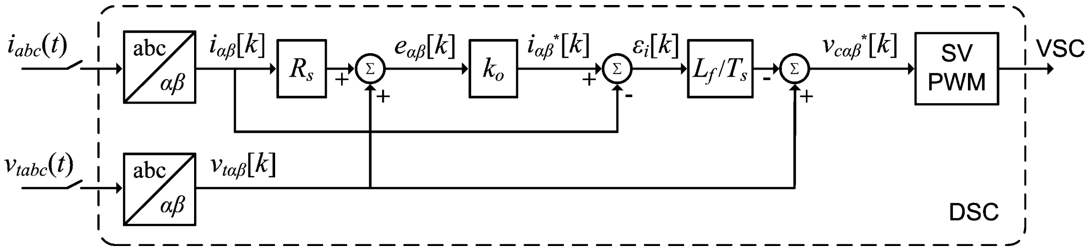

Fig. 7 Predictive control calculation and SV-PWM as implemented in the DSC.

tive itself, i.e. while the c-phase EMF is still zero. This current can be seen to be 180° out of phase with the terminal voltage during this time and therefore only constitutes losses. As the c-phase becomes active, the current and terminal voltage can be seen to track the EMF. The current is in phase with the EMF as required. The terminal voltage is also in phase with the EMF

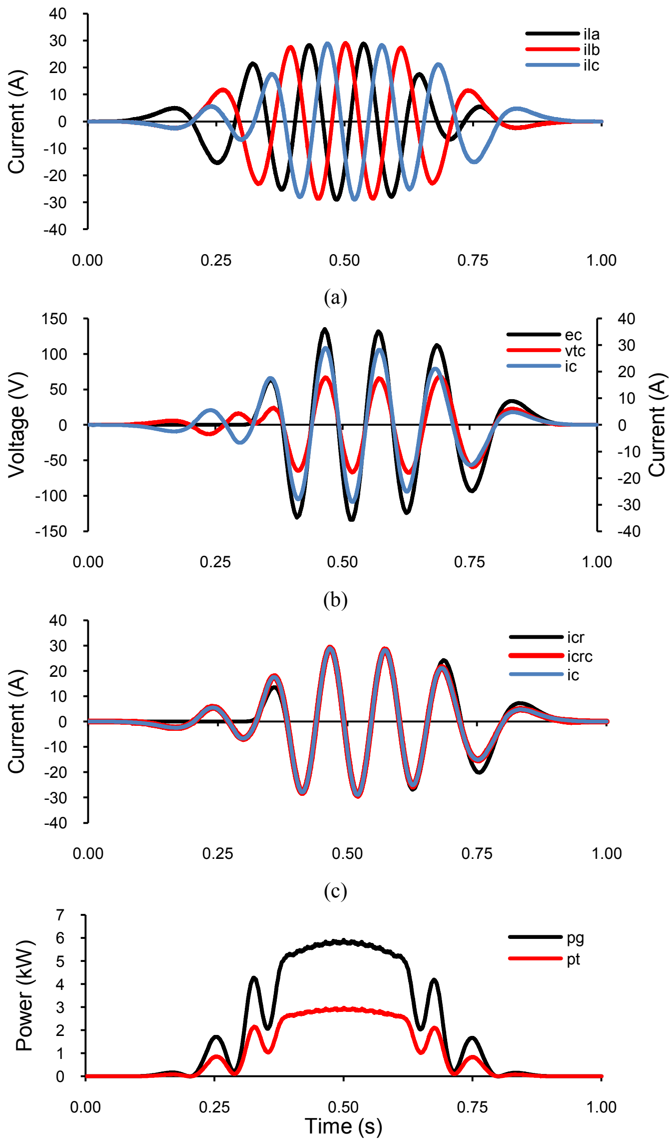

(d)

Fig. 8. Simulation under optimal current control conditions yields (a) the three phase currents injected to the converter; (b) c-phase emf (e_c), terminal voltage (v_{tc}) and current (i_c); (c) c-phase ideal reference current (i_{cr}), reference current as calculated in the control (i_{crc}) and the simulated current (i_c); and (d) the three phasegenerated power (p_g) and the power injected to the converter (p_t).

and highlights the small effect of the synchronous inductance.

The c-phase current (i_c) is shown in Fig. 8(c) together with the ideal reference current (i_{cr}), as scaled from the known EMF, and the reference current (i_{crc}) calculated in the control algorithm from (5)-(6). The return currents from the a and b-phase during the start of the stroke cause the calculated reference to deviate from the ideal reference. The simulated current follows the calculated reference current almost exactly.

The instantaneous three phase power generated (p_g) and transferred (p_t) from the LG is shown in Fig. 8(d). The dips in power at the beginning and end of the strokes can be contributed to the losses due to the circulation currents discussed before. The efficiency is 50 % with the rms power transferred to the converter calculated to be 1 kW. However, under these conditions 1 kW would also be dissipated as heat inside the machine, which would be unacceptable, as mentioned before. Setting $k_o = k_r =$ 0.074 in the control results in the rated current (as given in Table I) being drawn. Repeating the simulation now results in a average power of 580 W transferred to the converter at an efficiency of 83 %.

TABLE I. LG AND VSC PARAMETERS.

LG rated rms power P_g	1 kW	Filter inductance L_f	1.3 mH
LG rated peak EMF E_p	128 V	Filter capacitor C_f	23.5 µF
LG rated peak current I_p	9.5 A	DC-bus voltage V_d	300 V
Phase resistance R_s	2.31 Ω	Switching frequency f_s	20 kHz
Phase reactance X_s (max)	0.47 Ω	Optimal scaling factor k_o	0.216
LG rated efficiency	85 %	Rated scaling factor k_r	0.074

VI. TEST RESULTS

A Texas Instruments TMS320F28335 32-bit floating point digital signal controller (DSC) is used to implement the control and SV-PWM calculations. Apart from the LG control, a normal field-oriented control algorithm for controlling the drive motor speed is also implemented. The drive motor is fitted with a resolver which enables position feedback necessary for dq-transformation of the motor currents. The outer speed control loop provides a q-axis current reference to the inner current control loop; the d-axis current reference is kept equal to zero. Controlling the drive motor speed at a constant value while the LG is on load is necessary to reproduce the simulated conditions as closely as possible.

At the time of measurement, some mechanical problems were experienced with the drive system which prevented testing at rated conditions. A current scaling factor of k = 0.023 was used to produce the measured three phase currents shown in Fig. 9(a). The wave shapes clearly correspond very well with those of Fig 8(a). In Fig. 9(b) the measured a-phase current is shown together with the simulated current for the same conditions. Very good agreement between the two is observed. The

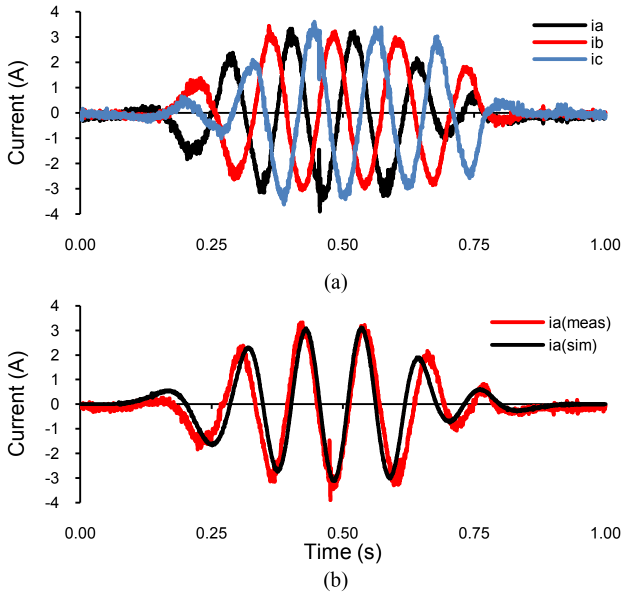

Fig. 9 Measurements with $k = 0.023$ showing (a) the three phase currents as injected to the VSC and the (b) measured and simulated *a*-phase current.

phase shift between the measured and simulated waveform at times is due to the fact that the drive motor speed cannot be controlled exactly constant during the stroke. The current is also in phase with the terminal voltage (not shown). The test results show that the predictive control works correctly, even though optimal and rated conditions could not be tested.

VII. Conclusion

The conclusions derived from the work presented in this paper can be summarized as follows:

1. Zero overlap between the stator and translator at the stroke ends of LGs can improve the generated energy per translator mass/cost compared to LGs designed for full stator – translator overlap during the entire stroke. In this particular case a 46 % increase was found, although it must be mentioned that the stroke length of the LG of this paper was not designed for actual wave heights.
2. Predictive control of the LG output is demonstrated, through simulation and measurement results, as an effective means of achieving optimal power transfer between a LG and its load without the need for linear position feedback or EMF estimation with sense coils.
3. The low synchronous inductance of the air-cored LG and the low operating frequency results in a near-unity power factor for the LG and therefore good efficiency.
4. In this particular LG, during the beginning and ending of the stroke when there is only partial overlap between the stator and translator, transition phase currents flow in some of the phases with zero back EMF which causes unwanted losses. Referring back to the first conclusion, the energy per translator mass/cost is still better than for total stator–translator overlap.

References

[1] A. F. d. O. Falcão, "Wave energy utilisation: A review of the technologies," *Renew. and Sust. Energy Rev.*, vol. 14, pp. 899-918, 2010.

[2] H. Polinder, M. E. C. Damen, and F. Gardner, "Linear PM generator system for wave energy conversion in the AWS," *IEEE Trans. Energy Convers.*, vol. 19, no. 3, pp. 583-589, Sep. 2004.

[3] P. C. J. Clifton, R. A. McMahon, and H. P. Kelly, "Design and commissioning of a 30 kW direct drive wave generator," in *Proc. IET 5th Int. Conf. Power Electron., Mach. and Drives*, Brighton, UK, 2010, p. 6.

[4] J. Prudell, M. Stoddard, E. Amon, T. K. A. Brekken, and A. von Jouanne, "A permanent-magnet tubular linear generator for ocean wave energy conversion," *IEEE Trans. Ind. Appl.*, vol. 46, no. 6, pp. 2392-2400, Nov. 2010.

[5] O. Danielsson, M. Eriksson, and M. Leijon, "Study of a longitudinal flux permanent magnet linear generator for wave energy converters," *Int. J. Energy Research*, vol. 30, pp. 1130-1145, May 2006.

[6] M. A. Mueller, N. J. Baker, L. Ran, N. G. Chong, H. Wei, P. J. Tavner, P. McKeever, "Experimental tests of an air-cored PM tubular generator for direct drive wave energy converters," in *Proc. IET 4th Int. Conf. Power Electron., Mach. and Drives*, York, UK, 2008, pp. 747-751.

[7] N. Hodgins, O. Keysan, A. McDonald, and M. Mueller, "Linear Generator for Direct Drive Wave Energy Applications," in *Proc. Int. Conf. Elect. Mach.*, Rome, Italy, 2010, p. 6.

[8] R. Vermaak and M. J. Kamper, "Design of a novel air-cored permanent magnet linear generator for wave energy conversion," in *Proc. Int. Conf. Elect. Mach.*, Rome, Italy, 2010, p. 6.

[9] J. K. H. Shek, D. E. Macpherson, and M. A. Mueller, "Experimental verification of linear generator control for direct drive wave energy conversion," *IET Renew. Power Gen.*, vol. 4, no. 5, pp. 395-403, 2010.

[10] B. Das and B. C. Pal, "Voltage control performance of AWS connected for grid operation," *IEEE Trans. Energy Convers.*, vol. 21, no. 2, pp. 353-361, Jun. 2006.

[11] K. Thorburn and M. Leijon, "Farm size comparison with analytical model of linear generator wave energy converters," *Ocean. Eng.*, vol. 34, pp. 908-916, 2007.

[12] D. O'Sullivan and G. Dalton, "Challenges in the grid-connection of wave energy devices," in *European Wave and Tidal Energy Conf.*, Uppsala, Sweden, 2009, pp. 12-20.

[13] P. R. M. Brooking and M. A. Mueller, "Power conditioning of the output from a linear vernier hybrid permanent magnet linear generator for use in direct drive wave energy converters," *IEE Proc.-Gener. Transm. Distrib.*, vol. 152, no. 5, pp. 673-681, Sep. 2005.

[14] V. D. Colli, P. Cancelliere, F. Marignetti, and R. Di Stefano, "A tubular-generator drive for wave energy conversion," *IEEE Trans. Ind. Electron.*, vol. 53, no. 4, pp. 1152-1159, Aug. 2006.

[15] J. K. H. Shek, D. E. Macpherson, M. A. Mueller, and J. Xiang, "Reaction force control of a linear electrical generator for direct drive wave energy conversion," *IET Renew. Power Gener.*, vol. 1, no. 1, pp. 17-24, 2007.

[16] F. Wu, X.-P. Zhang, P. Ju, and M. J. H. Sterling, "Optimal control for AWS-based wave energy conversion system," *IEEE Trans. Power Syst.* vol. 24, no. 4, pp. 1747-1755, Nov. 2009.

[17] L. Ran, M. A. Mueller, C. Ng, P. J. Tavner, H. Zhao, N. J. Baker, S. McDonald and P. McKeever, "Power conversion and control for a linear direct drive permanent magnet generator for wave energy," *IET Renew. Power Gener.*, vol. 5, no. 1, pp. 1-9, 2011.

[18] O. Danielsson and M. Leijon, "Flux distribution in linear permanent magnet synchronous machines including longitudinal end effects," *IEEE Trans. Magn.*, vol. 43, no. 7, pp. 3197-3201, Jul. 2007.

[19] L. Malesani, P. Mattavelli, and S. Buso, "Robust dead-beat current control for PWM rectifiers and active filters," *IEEE Trans. Ind. Appl.*, vol. 35, no. 3, pp. 613-620, May 1999.

[20] G. H. Bode, P. C. Loh, M. J. Newman and D. G. Holmes, "An improved robust predictive current regulation algorithm," *IEEE Trans. Ind. Appl.*, vol. 41, no. 6, pp. 1720-1733, Nov. 2005.

[21] H. W. van der Broeck, H.-C. Skudelny and G. V. Stanke, "Analysis and realization of a pulswidth modulator based on voltage space vectors," *IEEE Trans. Ind. Appl.*, vol. 24, no. 1, pp. 142-150, Jan. 1988.

[22] P. J. Randewijk, "Multi-domain system simulation and rapid prototyping of digital control algorithms using VHDL-AMS," in *Proc. IEEE Int. Conf. Power Electron. & Drive Syst.*, Bangkok, Thailand, 2007, p. 8.